NANO LETTERS

Letter

pubs.acs.org/NanoLett

Nature of the Metal Insulator Transition in Ultrathin Epitaxial Vanadium Dioxide

N. F. Quackenbush,[†] J. W. Tashman,[‡] J. A. Mundy,[§] S. Sallis,[∥] H. Paik,[‡] R. Misra,[⊥] J. A. Moyer,[¶] J.-H. Guo,[#] D. A. Fischer,[■] J. C. Woicik,[■] D. A. Muller,[§,Δ] D. G. Schlom,[‡,Δ] and L. F. J. Piper*[,†,∥]

[†]Department of Physics, Applied Physics and Astronomy, Binghamton University, Binghamton, New York 13902, United States

[‡]Department of Materials Science and Engineering, Cornell University, Ithaca, New York 14853-1501, United States

[§]School of Applied and Engineering Physics, Cornell University, Ithaca, New York 14853, United States

[∥]Materials Science and Engineering, Binghamton University, Binghamton, New York 13902, United States

[⊥]Department of Physics and Materials Research Institute, Pennsylvania State University, University Park, Pennsylvania, 16802, United States

[¶]Department of Physics, University of Illinois at Urbana−Champaign, Urbana, Illinois 61801, United States

[#]Advanced Light Source, Lawrence Berkeley National Laboratory, Berkeley, California, United States

[■]Materials Science and Engineering Laboratory, National Institute of Standards and Technology, Gaithersburg, Maryland 20899, United States

[Δ]Kavli Institute at Cornell for Nanoscale Science, Ithaca, New York 14853, United States

Supporting Information

ABSTRACT: We have combined hard X-ray photoelectron spectroscopy with angular dependent O K-edge and V L-edge X-ray absorption spectroscopy to study the electronic structure of metallic and insulating end point phases in 4.1 nm thick (14 units cells along the *c*-axis of VO_2) films on TiO_2(001) substrates, each displaying an abrupt MIT centered at ∼300 K with width <20 K and a resistance change of $\Delta R/R > 10^3$. The dimensions, quality of the films, and stoichiometry were confirmed by a combination of scanning transmission electron microscopy with electron energy loss spectroscopy, X-ray spectroscopy, and resistivity measurements. The measured end point phases agree with their bulk counterparts. This clearly shows that, apart from the strain induced change in transition temperature, the underlying mechanism of the MIT for technologically relevant dimensions must be the same as the bulk for this orientation.

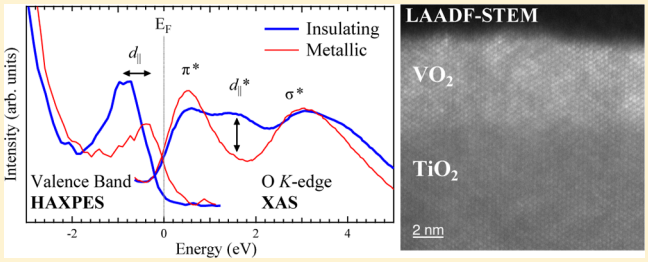

KEYWORDS: *VO_2, metal insulator transition, X-ray spectroscopy, transition metal oxides, ultrathin films*

Transition metal oxides that display abrupt phase transitions are considered a promising approach to continuing advances in information processing and storage beyond current CMOS scaling.[1] Vanadium dioxide (VO_2) has been an exquisite textbook example of an abrupt metal insulator transition (MIT) for the last five decades with its ultrafast (typically picosecond or less) and large (∼10^4) discontinuity in its resistivity at 340 K (bulk VO_2).[2] By lowering the temperature from the high-temperature rutile metallic phase, a structural phase transition (SPT) accompanies the MIT resulting in a low-temperature monoclinic insulating phase.[3,4] The interplay of the electron correlation (Mott transition) and the lattice (Peierls instability) of VO_2 gives rise to rich physics.[5−8] For instance, the phase transition of VO_2 can be induced by thermal,[2] electrical,[9,10] optical,[11] and strain triggering,[12,13] which makes it highly appealing for a variety of novel switching devices.[14]

Charged defects and the multiple valence states possible for vanadium means that nonstoichiometric V_yO_x can display a startlingly complex phase diagram with VO_2 stable within a slim region of phase space.[15] Recent advances in the preparation of high-quality nanorods of VO_2 have largely circumvented issues associated with thin films, which typically exhibit misfit dislocations and grain boundaries,[16] facilitating studies regarding the effects of coherent strain on the MIT.[13,17−20] High-quality homogeneous ultrathin films rather than nanorods are, however, ultimately desired for two terminal VO_2 devices, which utilize an electric field (or Joule heating) driven MIT for nonlinear *I*−*V* switching electronics.[9,14,21,22] The realization of novel switching devices employing VO_2 demands studies of

Received: July 22, 2013
Revised: September 2, 2013
Published: September 3, 2013

high quality epitaxial ultrathin (≤10 nm) films in order to disentangle materials quality issues from the intrinsic properties of nanoscale films.

A key issue for such scaled devices is the nature of the MIT and whether it persists at these ultrathin dimensions. Recently, Kar et al. provided the first systematic scaling of switching characteristics of homogeneous ultrathin VO_2 films down to 10 nm and stressed the importance of coexisting domains during the transition inferred from the $I-V$ and impedance spectroscopy analysis.[22] Determining the exact nature of these phases requires powerful X-ray spectroscopy and scattering techniques that are the benchmark for theoretical studies of nature of the MIT[4,6,23,24] but have have largely been restricted to bulk crystals of VO_2.[6,7,25,26] X-ray spectroscopic studies of the electronic structure of these phases at dimensions approaching 1 nm are necessary for further providing valuable information regarding both the fundamental nature of the MIT for confined films and the ultimate scaling limits of VO_2 for devices.

In this Letter, we have studied at room temperature the insulating and metallic end point phases of epitaxial VO_2 4.1 nm (14 units cells along the c-axis) thick grown on TiO_2(001) substrates. The dimensions, quality of the films, and stoichiometry were confirmed by a combination of scanning transmission electron microscopy with electron energy loss spectroscopy (STEM-EELS), X-ray spectroscopy, and resistivity measurements. The corresponding occupied and unoccupied density of states (DOS) of the end point phases were measured using spatially averaging hard X-ray photoelectron spectroscopy (HAXPES) and V $L_{3,2}$- and O K-edge angular X-ray absorption spectroscopy (XAS), respectively. HAXPES and XAS are employed to circumvent the need for surface preparation, since typical surface preparation techniques such as ion bombardment or even mild annealing can result in vanadium reduction giving rise to a complex mixture of V_yO_x surface oxides.[27,28] Complementary, more surface sensitive, X-ray photoelectron spectroscopy (XPS) measurements using a lower photon energy were also performed. We show that this approach can be used to distinguish contributions from the VO_2 overlayer and TiO_2 substrate for films approaching 1 nm in thickness. Our results confirm that apart from the strain-induced change in transition temperature, the underlying MIT mechanism for technologically relevant dimensions must be the same as the bulk for this strained orientation.

Figure 1 displays the resistivity measurements of two ultrathin VO_2 samples, which both show abrupt MITs, that is, width <20 K and a resistance (R) change of $\Delta R/R > 10^3$. The hysteresis loops are centered at ∼292.5 and ∼304 K for Sample A and Sample B, respectively. An additional 6 min anneal was applied to Sample A following the growth, which may account for the sharper hysteresis loop and lower transition temperature compared to Sample B. At room temperature, samples A and B were found to be in their respective metallic and insulating end point phases. This facilitated the investigation of both phases consecutively at room temperature.

In order to both verify the film thickness and film quality (especially at the interface) we employed STEM-EELS, as shown in Figure 2. The atomic similarity of the TiO_2 substrate and VO_2 substrate results in poor contrast in the high-angle annular dark field (HAADF) mode STEM, so the results presented here are low-angle annular dark field (LAADF) STEM. From analysis of the corresponding EELS of the V $L_{3,2}$-edge we obtained 13.2 (14.6) unit cells using the total V (full

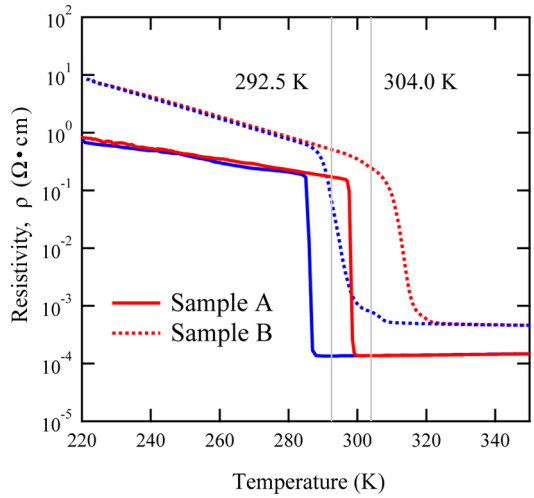

Figure 1. The temperature-dependent resistivity plots of the two VO_2 samples. Vertical thin gray lines indicate the center of the hysteresis loops for both samples.

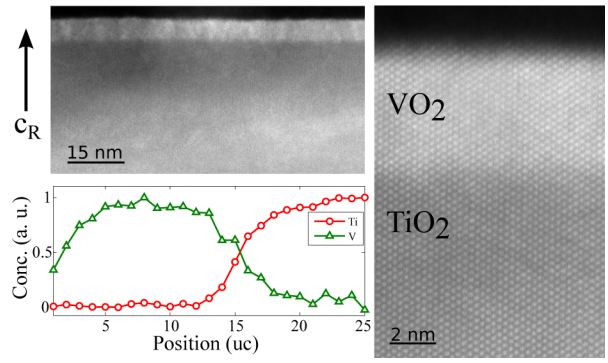

Figure 2. The LAADF-STEM images of Sample A at different magnifications, the c_R-axis direction is indicated alongside. Also shown is the Ti and V L-edge EELS signal as a function of unit cell (uc) thickness.

width at half-maximum) signal, which corresponded well to 14 unit cells from the growth rate. The V L-edge (Supporting Information) displayed the characteristic V^{4+} line shape.[29] Depth profiles of the V and Ti $L_{3,2}$-edge EELS signals reveals Ti interdiffusion restricted to within 3−4 unit cells at the interfaces. The severe weakening of the MIT for films below 7 nm has been attributed to Ti interdiffusion at the interface.[30] The abrupt nature of the MIT in our films provides an upper limit regarding the amount of interdiffusion that may be tolerated with ultrathin films. At the other end (i.e., the surface), there is a reduction of the V signal. This is attributed to an over oxidized surface layer. This is consistent with our XPS which displayed a V^{5+} contribution in the V 2p core-level region localized to the topmost layers (refer to Supporting Information).

We employed both surface-sensitive and bulk-sensitive modes of XAS using the total electron yield (TEY) and total fluorescent yield modes (TFY) in order to distinguish contributions from the epilayer, substrate, and interfaces. Our analysis of angular XAS of ultrathin oxide epilayers on oxide substrates has revealed that the TEY signal is representative of up to ∼1−5 nm of material, while TFY has an effective probing depth of ∼10−100 nm depending on angle, which qualitatively matches expectations.[31] Our angular measurements revealed

dx.doi.org/10.1021/nl402716d | Nano Lett. 2013, 13, 4857−4861

the same V L-edge profile in both modes confirming a uniform film consistent with the STEM-EELS results. The TEY mode spectra was only associated with the VO_2 epilayer (refer to Supporting Information). Only the TFY mode O K-edge XAS displayed contributions from both layers that varied with angle, with the TiO_2 signal providing an internal energy reference for our measurements. Figure 3 displays the angular variation of

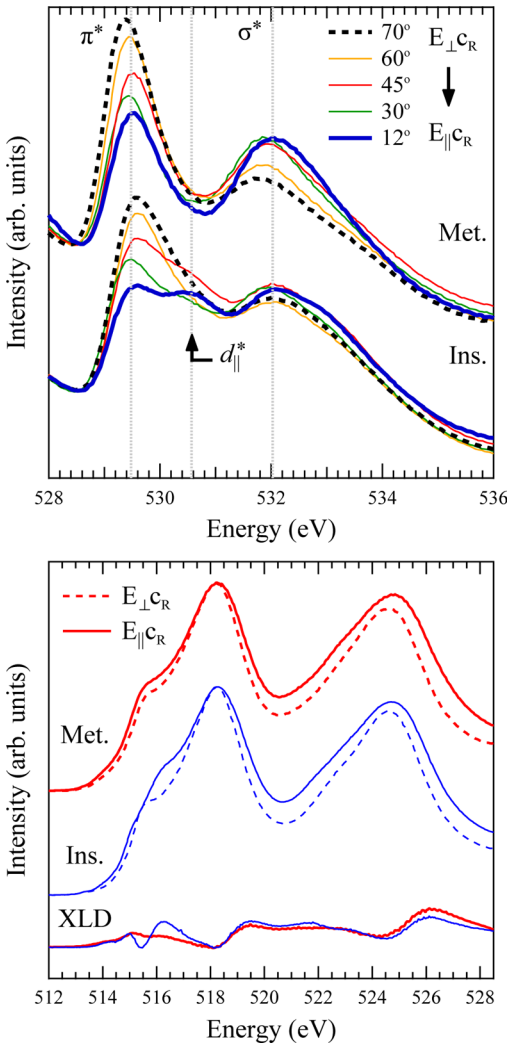

Figure 3. (Top) Angular-dependent O K-edge XAS spectra of VO_2(001) in both the metallic and insulating phases, showing the evolution of the $d_{\|}$ state. (Bottom) Linear X-ray dichroism of the V $L_{3,2}$-edge XAS of the metallic and insulating end points.

the V $L_{3,2}$ and O K-edge XAS. The strict dipole selection rules and energy constraints of XAS ensures that one can obtain elemental and orbital selectivity. In the case of the O K-edge (1s → 2p*), XAS measures the O 2p partial density of states (PDOS) above the Fermi level. Whereas the stronger atomic overlap between the p and d orbitals means that the metal $L_{3,2}$ edge (2p → 3d*) XAS reflects the spectra associated with transitions between the $2p^63d^n$ initial and $2p^53d^{n+1}$ final state multiplets and is therefore an excellent indicator of oxidation state. We assign spectral features in the O K-edge region (~525−545 eV) as associated with the π^* (~530 eV) and σ^* (~532 eV) states. An additional $d_{\|}^*$ orbital appears only in the insulating phase at certain angles. This is consistent with reports of VO_2 elsewhere[7,32,33] and is discussed further below.

The peak energy and spectral shape of the V L_3-edge region (~510−522) is in agreement with the V^{4+} charge state of VO_2,[6] consistent with the STEM-EELS in Figure 2. Our angular dichroism in both the TEY and TFY modes of the V $L_{3,2}$-edge spectra confirms the shift from 3D orbital character in the metallic phase to 1D orbital character in the insulating phase, observed for bulk crystals.[6] Here, any V^{5+} contribution from the oxidized overlayer was found to be dwarfed by the epilayer signal the V L_3-edge region.

The corresponding HAXPES and XPS of the valence band region for the two end point phases are shown in Figure 4. The

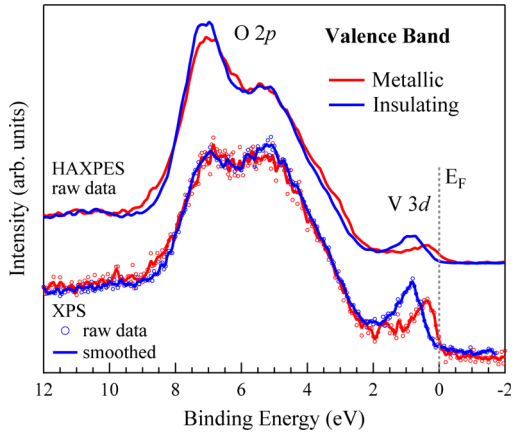

Figure 4. The HAXPES and XPS of the valence band region of our two ultrathin samples at room temperature referenced to the Fermi level E_F. A 1-point smooth has been applied to the XPS due to the lower count rate associated with the attenuating overlayer.

topmost V 3d (0−2 eV) states display a clear shift between the insulating and metallic phases, consistent with the respective bulk end point phases of VO_2.[7,34] It is important to note that for the XPS no surface preparation was performed, which confirms a robust MIT extending to the surface. The attenuation profile of the photoelectrons at this photon energy means that the majority of our signal comes from within the first nanometer. The O 1s and V 2p core-level regions are shown in the Supporting Information. The greatest difference between the HAXPES and XPS, apart from intensity and orbital cross-section variation, is the appearance of a V^{5+} contribution due to the overoxidized topmost atomic layers evident in the XPS data, due to the aforementioned surface sensitivity of the measurement. The corresponding work-function from Kelvin probe measurements of the two samples were 5.16 eV (insulating) and 5.3 eV (metallic), consistent with the energetic shift reported by Ramanathan et al.[35]

We now discuss our results within the context of the molecular orbital model proposed by Goodenough.[3,4] Figure 5 displays the high-temperature rutile (R) and low-temperature monoclinic (M_1) crystal structures with their corresponding molecular orbital diagrams. The lowering of the crystal symmetry from rutile to monoclinic lifts the orbital degeneracy. The formation of the V−V dimers along the rutile c- (c_R) axis splits the nonbonding $d_{\|}$ states into occupied and unoccupied states. Meanwhile the zigzagging of the V−V pairs shifts the π^* state to higher energies, opening the band gap in the M_1 phase.

Referring to Figure 3, the O K-edge spectra of the metallic phase displayed only two distinct features associated with the π^* and σ^* peaks consistent with this model. As the angle of the c_R-axis of the rutile phase is varied with respect to the electric

dx.doi.org/10.1021/nl402716d | Nano Lett. 2013, 13, 4857−4861

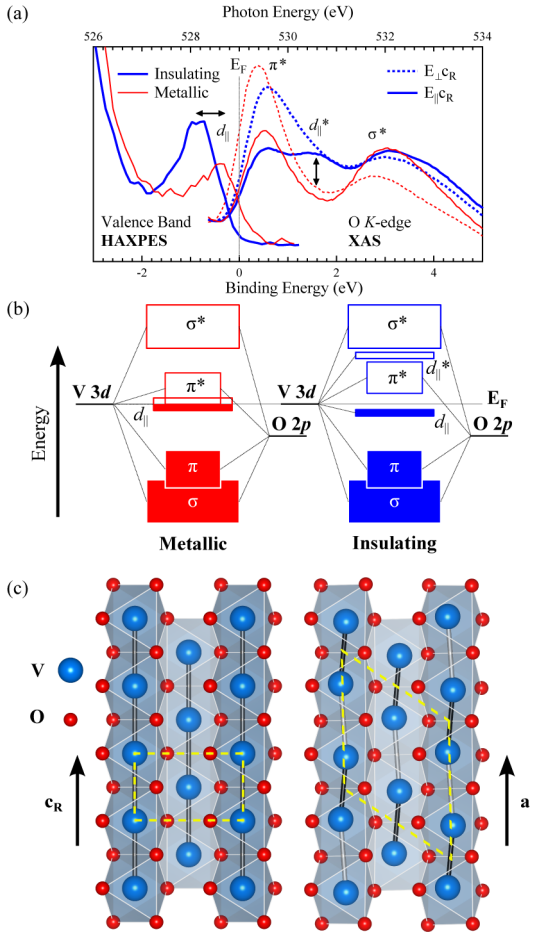

Figure 5. (a) The HAXPES and O K-edge spectra of the end point phases on a common binding energy plot, referenced to the Fermi level (E_F). (b) The molecular orbital diagram for the insulating and metallic phases. (c) The corresponding rutile (R) and monoclinic (M_1) crystal structures of the end point phases of VO_2. The unit cells are shown (dashed yellow lines) to indicate the effective doubling of the M_1 cell compared to the R phase.

field (E) of the incoming X-rays, the relative intensities of the two peaks change. In the insulating phase the same variation is noted. Note that the c_R-axis corresponds to the direction of the V−V dimer chains in the M_1 phase, as shown in Figure 5. The unoccupied $d_{\parallel}^*$ state is observed at 530.8 eV and becomes pronounced as the E becomes more closely aligned with the c_R-axis, consistent with its orbital character.[7,32,33] In addition, we clearly observe the corresponding 0.15−0.2 eV shift in the π^* peak upon going into the insulating phase, which is attributed to the zigzagging of the V−V pairs. The XAS measurements of the two samples were measured consecutively at each angle to rule out any artificial shifts in our analysis associated with geometry and photon energy. The energetic separation between the π^* and the $d_{\parallel}^*$ was found to be 0.9 eV, in agreement with the bulk phase.[7] Recent XAS of 40 nm strained film on TiO_2(001) and dynamical mean field theory (DMFT) have confirmed that for the strain associated with the (001) orientation the splitting should be the same as in the bulk phase.[23,33] Our result is then consistent with thicker strained films in this orientation despite being an order of magnitude thinner.

Furthermore, we have combined the HAXPES and the O K-edge XAS on a common energy axis for direct comparison with the molecular orbital diagram in Figure 5. The energy alignment of the HAXPES and the O K-edge XAS was first ensured by shifting the measured energy of the XAS by the O 1s core-level resulting in a plot on a common binding energy axis referenced to the Fermi level. Following this shift, the XAS onset is shown to lie below the Fermi level because the final state of XAS has a core-hole which effectively shifts the absorption spectrum to lower energies.[36] For the O K-edge XAS, applying a 1 eV shift is usually adequate for direct comparison with DFT;[37] applying this approximation agrees well with the band edge separation for both the metallic and insulating phases. This approach facilitates direct comparison with the calculated DOS from combined local density approximation of density functional theory incorporated with dynamical mean field theory (LDA-DMFT) of strained thin films by Kotliar et al.[23] In the insulating phase, we observe an energetic separation between the $d_{\parallel}$ states of 2.2 eV, which agrees well with 2.15 eV for the LDA-DMFT calculated splitting of the $d_{x^2-y^2}$ orbital for the strained VO_2 films on TiO_2(001).[23]

In conclusion, we have combined HAXPES and angular XAS to circumvent issues associated with surface preparation to study the scaling properties of ultrathin VO_2. We confirmed that our ultrathin films were 4.1 nm (14 units cells along the c-axis) in thickness, had Ti interdiffusion restricted to 4 unit cells of the interface, and displayed abrupt MIT transitions at room temperature. The insulating and metallic end point phases spectroscopically agree with their bulk counterparts, indicating that apart from the strain-induced change in transition temperature, the underlying mechanism of the MIT for technologically relevant dimensions must be the same as the bulk for this orientation in agreement with LDA-DMFT. Our results suggest that the scaling of functional VO_2 to the single nanometer regime can be realized.

Methods. The films of 4.1 nm (14 units cells along the c-axis) VO_2 were grown on 0.5 mm thick TiO_2 via reactive oxide molecular-beam epitaxy (MBE) at 400 °C. HAXPES measurements were performed at beamline X24a of the National Synchrotron Light Source (NSLS), using a photon energy of ~4 KeV. Laboratory based XPS using a monochromatic Al K_α source was performed at Binghamton University set to the same effective instrumental resolution. Angular soft XAS measurements were performed at AXIS endstation at beamline 7 of the Advanced Light Source (ALS).

■ ASSOCIATED CONTENT

Supporting Information

The following items are included in the supplemental section: (1) an evaluation of the effective probing depth of TEY and TFY mode XAS; (2) the V L_3-edge EELS spectra; (3) an evaluation of V charge state as a function of film thickness using HAXPES and XPS survey and core-level scans of VO_2; and (4) the change in O 1s and V 2p lineshapes between metallic and insulating phases using HAXPES and XPS. This material is available free of charge via the Internet at http://pubs.acs.org.

■ AUTHOR INFORMATION

Corresponding Author

*E-mail: lpiper@binghamton.edu.

Notes

The authors declare no competing financial interest.

dx.doi.org/10.1021/nl402716d | Nano Lett. 2013, 13, 4857−4861

■ ACKNOWLEDGMENTS

The authors thank Peter Schiffer for transport measurements within his laboratory. Acknowledgment is made to the Donors of the American Chemical Society Petroleum Research Fund for support (or partial support) of this research. Additional support (L.F.J.P) was provided by an Analytical and Diagnostics Laboratory Small Grant program at Binghamton. The NSLS is supported by the U.S. Department of Energy, Office of Science, Office of Basic Energy Sciences, under Contract No. DE-AC02-98CH10886. L.F.J.P., N.F.Q., and S. S. acknowledge support from the Faculty/Student Research Support Program at the NSLS. Beamline X24a at the NSLS is supported by the National Institute of Standards and Technology. The Advanced Light Source is supported by the Director, Office of Science, Office of Basic Energy Sciences, of the U.S. Department of Energy under Contract No. DE-AC02-05CH11231. J.W.T., H.P., and D.G.S. acknowledge the financial support of ONR through award N00014-11-1-0665. J.A.M. acknowledges support from the A.R.O in the form of a NDSEG fellowship and from the NSF in the form of a GRFP fellowship. This work was supported as part of the Energy Materials Center at Cornell (EMC2), an Energy Frontier Research Center funded by the U.S. Department of Energy, Office of Science, Office of Basic Energy Sciences under Grant DE-SC0001086. This work also made use of the electron microscopy facility of the Cornell Center for Materials Research (CCMR) supported by the National Science Foundation under Award Number DMR-1120296.

■ REFERENCES

(1) Takagi, H.; Hwang, H. Y. *Science* **2010**, *327*, 1601.
(2) Morin, F. J. *Phys. Rev. Lett.* **1959**, *3*, 34.
(3) Goodenough, J. B. *J. Solid State Chem.* **1971**, *3*, 490.
(4) Eyert, V. *Ann. Phys.* **2002**, *11*, 650.
(5) Biermann, S.; Poteryaev; Lichtenstein, A.; Georges, A. *Phys. Rev. Lett.* **2005**, *94*, 026404.
(6) Haverkort, M. W.; Hu, Z.; Tanaka, A.; Reichelt, W.; Streltsov, S.; Korotin, M. A.; Anisimov, V. I.; Hsieh, H. H.; Lin, H.-J.; Chen, C. T.; Khomskii, D. I.; Tjeng, L. H. *Phys. Rev. Lett.* **2005**, *95*, 196404.
(7) Koethe, T. C.; Hu, Z.; Haverkort, M.; Schussler-Langeheine, C.; Venturini, F.; Brookes, N. B.; Tjernberg, O.; Reichelt, W.; Hsieh, H. H.; Lin, H.-J.; Chen, C. T.; Tjeng, L. H. *Phys. Rev. Lett.* **2006**, *97*, 116402.
(8) Qazilbash, M. M.; Brehm, M.; Chae, B.-G.; Ho, P.-C.; Andreev, G. O.; Kim, B.-J.; Yun, S. J.; Balatsky, A. V.; Maple, M. B.; Keilmann, F.; Kim, H.-T.; Basov, D. N. *Science* **2007**, *318*, 1750.
(9) Stefanovich, G.; Pergament, A.; Stefanovich, D. *J. Phys.: Condens. Matter* **2000**, *12*, 8837.
(10) Nakano, M.; Shibuya, K.; Okuyama, D.; Hatano, T.; Ono, S.; Kawasaki, M.; Iwasa, Y.; Tokura, Y. *Nature* **2012**, *487*, 459.
(11) Cavalleri, A.; Toth, C.; Siders, C. W.; Squier, J. A.; Raski, F.; Forget, P.; Kieffer, J. C. *Phys. Rev. Lett.* **2001**, *87*, 237401.
(12) Muraoka, Y.; Hiroi, Y. *Appl. Phys. Lett.* **2002**, *80*, 583.
(13) Cao, J.; Ertekin, E.; Srinivasan, V.; Fan, W.; Huang, S.; Zheng, H.; Yim, J. W. L.; Khanal, D. R.; Ogletree, D. F.; Grossman, J. C.; Wu, J. *Nat. Nanotechnol.* **2009**, *4*, 732.
(14) Yang, Z.; Ko, C.; Ramanathan, S. *Annu. Rev. Mater. Res.* **2011**, *41*, 337.
(15) Katzke, H.; Toledano, P.; Depmeier, W. *Phys. Rev. B* **2003**, *68*, 024109.
(16) Natelson, D. *Nat. Nanotechnol.* **2009**, *4*, 406.
(17) Jiang Wei, W. C.; Wang, Z.; Cobden, D. H. *Nat. Nanotechnol.* **2009**, *4*, 420.
(18) Zhang, S.; Chou, J. Y.; Lauhon, L. J. *Nano Lett.* **2009**, *9*, 4527.
(19) Cao, J.; Gu, Y.; Fan, W.; Chen, L. Q.; Ogletree, D. F.; Chen, K.; Tamura, N.; Kunz, M.; Barrtt, C.; Seidel, J.; Wu, J. *Nano Lett.* **2010**, *10*, 2667.
(20) Zhang, S.; Kim, I. S.; Lauhon, L. J. *Nano Lett.* **2011**, *11*, 1443.
(21) Gopalakrishnan, G.; Ruzmetov, D.; Ramanathan, S. *J. Mater. Sci.* **2009**, *44*, 5345.
(22) Kar, A.; Shukla, N.; Freeman, E.; Paik, H.; Liu, H.; Engle-Herbert, R.; D. G. Schlom, S. S. N. B.; Datta, S. *Appl. Phys. Lett.* **2013**, *102*, 072106.
(23) Lazarovits, B.; Kim, K.; Haule, K.; Kotliar, G. *Phys. Rev. B* **2010**, *81*, 115117.
(24) Eyert, V. *Phys. Rev. Lett.* **2011**, *107*, 016401.
(25) Corr, S. A.; Shoemaker, D. P.; Melot, B. C.; Seshadri, R. *Phys. Rev. Lett.* **2010**, *105*, 056404.
(26) Booth, J. M.; Casey, P. S. *Phys. Rev. Lett.* **2009**, *103*, 086402.
(27) Mendialdua, J.; Casanova, R.; Barbaux, Y. *J. Electron. Spectrosc. Relat. Phemon.* **1995**, *71*, 249−261.
(28) Silversmit, G.; Depla, D.; Poelman, H.; Marin, G. B.; Gryse, R. D. *J. Electron. Spectrosc. Relat. Phemon.* **2004**, *135*, 167−175.
(29) Fitting Kourkoutis, L.; Hotta, Y.; Susaki, T.; Hwang, H. Y.; Muller, D. A. *Phys. Rev. Lett.* **2006**, *97*, 256803.
(30) Muraoka, Y.; Saeki, K.; Eguchi, R.; Wakita, T.; Hirai, M.; Yokoya, T.; Shin, S. *J. Appl. Phys.* **2011**, *109*, 043702.
(31) Stohr, J. *NEXAFS Spectroscopy*; Springer Series in Surface Sciences; Springer: New York, 1992.
(32) Abbate, M.; deGroot, F. M. F.; Fuggle, J. C.; Ma, Y. J.; Chen, C. T.; Sette, F.; Fujimori, A.; Ueda, Y.; Kosuge, K. *Phys. Rev. B* **1991**, *43*, 7263.
(33) Laverock, J.; Piper, L. F. J.; Preston, A. R. H.; B. Chen, B.; McNulty, J.; Smith, K. E.; Kittiwatanakul, S.; Lu, J. W.; Wolf, S. A.; Glans, P. A.; Guo, J. H. *Phys. Rev. B* **2012**, *85*, 081104.
(34) Eguchi, R.; et al. *Phys. Rev. B* **2008**, *78*, 075115.
(35) Ko, C.; Ramanathan, Z. Y. S. *ACS Appl. Mater. Interfaces* **2011**, *3*, 3396.
(36) Zhang, L.; Schwertfager, N.; Cheiwchanchamnangij, T.; Lin, X.; Glans-Suzuki, P. A.; Piper, L. F. J.; Limpijumnong, S.; Luo, Y.; Zhu, J. F.; Lambrecht, W. R. L.; Guo, J. H. *Phys. Rev. B.* **2012**, *86*, 245430.
(37) Preston, A. R. H.; Ruck, B. J.; Piper, L. F. J.; DeMasi, A.; Smith, K. E.; Schleife, A.; Fuchs, F.; Bechstedt, F.; J., C.; Durbin, S. M. *Phys. Rev. B* **2008**, *78*, 155114.